The application of an electrochemical microflow reactor for the electrosynthetic aldol reaction of acetone to diacetone alcohol

The application of an electrochemical microflow reactor for the electrosynthetic aldol reaction of acetone to diacetone alcohol

Danny Pauwels[a], Bart Geboes[a], Jonas Hereijgers[a], Daniel Choukroun[a], Karolien De Wael[b], Tom Breugelmans[a]*

[a]*University of Antwerp, Research Group Advanced Reactor Technology, Universiteitsplein 1, 2610 Wilrijk, Belgium.*

[b]*University of Antwerp, Research Group Antwerp X-ray analysis, Electrochemistry and Speciation, Groenenborgerlaan 171, 2020 Antwerp, Belgium.*

**Corresponding Author: tom.breugelmans@uantwerpen.be*

Abstract

The design and application of an electrochemical micro-flow reactor for the aldol reaction of acetone to diacetone alcohol (DAA) is reported. The modular reactor could be readily disassembled and reassembled to change the electrodes, incorporate a membrane and remove possible obstructions. The productivity and efficiency was quantified. Using a platinum deposit as electrocatalyst or an inert glassy carbon electrode as working electrode, the maximum obtainable equilibrium concentration of ±15 m% was reached after a single pass up to a flow rate of 8 ml min^{-1}, yielding 0.57 g min^{-1} DAA (3.46 mmol cm^{-3} min^{-1}) at an efficiency of 0.33 g C^{-1} on platinum and 0.50 g min^{-1} (3.04 mmol cm^{-3} min^{-1}) at 1.20 g C^{-1} on glassy carbon. Note that no optimisation studies have been made in the present paper.

1. Introduction

The aldol reaction of acetone to diacetone alcohol (4-hydroxy-4-methyl-pentan-2-one) is an industrially important reaction since diacetone alcohol is both an interesting intermediary to products such as methyl isobutyl ketone as a useful end product (Keefe et al., 2005). Common applications include its usage as a solvent in varnishes, paints, thinners and cleaning compounds and it's considered to be an environmentally friendly alternative to other materials such as acetone due to its much lower volatility (Kirschner, 1994). In previous work the use of electrosynthesis as an alternative to the conventional chemical process was investigated (Pauwels

et al., 2016). This preliminary study showed that it was possible to produce DAA through electrosynthesis in a standard batch setup and obtain the same equilibrium concentration as the commercial fixed-bed reactors. In addition the selectivity towards DAA was very high, generally above 95 %. However, electrochemical batch reactors of the stirred-tank-reactor type suffer from inhomogeneities of the current distribution and mass- and heat transfer (Küpper et al., 2003). Employing a parallel plate electrode geometry yields a setup which provides a homogeneous current distribution (Küpper et al., 2003; Rode et al., 2008). Furthermore, the high selectivity of the electrochemically performed reaction and ease of operation offer an opportunity to perform the reaction in a continuous flow system. The combination of these two improvements can be achieved in a micro-flow system. The recent reinvention of microflow cells for electrochemical synthesis builds on a long history of flow cell design and electrochemical engineering in the laboratory and industry (Marshall and Walsh, 1985; Pickett, 1979; Pletcher and Walsh, 1990; Wendt and Kreysa, 1999) and can build upon the progress achieved in these domains. The advances in microfluidic reactor systems and the inherent advantages associated therewith make this an ideal application for this case.

The definition of the electrochemical microfluidic reactor as intended here, comprises electrochemical microsystems with characteristic dimensions in the millimetre and sub millimetre range, hence a small distance between the electrodes (Ziogas et al., 2009). The close proximity of the electrodes and often associated laminar flows lead to an intensification of the kinetics and mass transfer to the electrodes, resulting in higher yields and faster conversions (Green et al., 2014; Scialdone et al., 2011). Additionally, the laminar flow ensures a stable homogeneous flow which prevents partially dead volumes which result in loss in selectivity (Küpper et al., 2003). The small inter-electrode distance also allows operation with low concentrations or even in absence of supporting electrolyte at low cell voltages due to the coupling (overlapping) of the diffusion layers of both electrodes at sufficiently small distances (Horcajada et al., 2005; Paddon et al., 2006, 2002; Ziogas et al., 2009). Furthermore, due to the laminar flow, the mass transfer of species in the direction perpendicular to the electrode's surface is governed only by diffusion so that in a well-dimensioned setup, separation of reaction products is possible (opposed to coupling of the electrodes) without the addition of a membrane (Horii et al., 2007). The high specific interfacial area (electrode surface area to volume ratio) allows high conversions after a single pass (Watts et al., 2014). These aspects, combined with the advantages associated with the small dimensions, make microfluidic reactors well-suited for fast screening of operative parameters or process optimisation (Scialdone et al., 2014). The addition of the precise control of reactive intermediates that electrosyntheses can offer due to the control of the potential, have made the application of electrochemical microfluidic reactors a viable and noteworthy alternative to batch processes in synthesis chemistry. This is reflected in the increasing attention it receives in literature in recent years. The list of electrochemical

microreactors for continuous flow synthesis reported in literature is extensive. Several recent designs and their performance are covered in a comprehensive review by Watts et al. (Watts et al., 2014).

Microreactor setups are more commonly employed for fine chemicals or pharmaceuticals than for commodity chemicals since they are often associated with high capital and operating costs and small production capacities and thus they need products with a high added value to render them economically viable. However, due to the ease of scale-up and the increased selectivity and conversion which lead to a less intensive and less costly purification, the use of a microreactor setup can become industrially applicable for certain commodities or specialties such as diacetone alcohol. In this work the construction and application of a microfluidic system for the aldol reaction of acetone to diacetone alcohol is reported. Industrial viability and implementation requires a robust design with focus on the ease of operation and high rate of product formation. Therefore, the design is uncomplicated and is based on a parallel plate electrode arrangement where both electrodes directly face each other, separated by a single flow channel. All benefits of the microfluidic reactor are maintained while a simple, yet performant device is acquired. This type of reactor design for electrochemical synthesis with rectangular flow channels is a widely used design in both industrial and laboratory applications and has been characterised extensively (Rivera et al., 2015a, 2015b), demonstrating its viability.

The setup is validated by evaluating different configurations with varying reactor and reaction parameters. This is done by checking the flow and the mass transfer on the one hand and assessing the performance (maximum obtainable concentration and selectivity), production rate capacity (yield per unit of time and space time yield) and efficiency (in this work: yield per unit of charge) on the other hand. Calculating the dimensionless current efficiency requires knowledge of the exact reaction mechanism, which for this reaction is not known. As a measure for the apparent current efficiency the ratio of the yield to the charge passed in the cell is used as both are related through Faraday's law of electrolysis. The space time yield ρ_{ST} is calculated using the reactor volume over the electrode. The aforementioned figures of merit are always interpreted with respect to the electrode surface area and the specific interfacial area, as these parameters determine for a large part the cost of the construction of the reactor.

2. Experimental

2.1. Chemicals

Acetone (HPLC grade, 99.8+ %) was purchased from Chem-Lab (Belgium). The supporting electrolyte tetrabutylammonium perchlorate (n-Bu_4NClO_4, 99.0 %), potassium ferricyanide ($K_3[Fe(CN)_6]$), potassium ferrocyanide ($K_4[Fe(CN)_6]$) and sodium sulphate (Na_2SO_4) was purchased from Sigma-Aldrich (Belgium). The platinum plating solution (Platinum Q Salt® Pt 5Q) was obtained from Alfa Aesar (Germany). The ultrapure water (18.2 MΩ cm^{-1} at 25 °C) was prepared in the laboratory (Milli-Q, Millipore).

2.2. Design of the electrochemical microreactor

To be suitable for industrial implementation, the electrochemical microreactor has to meet certain design criteria besides the performance requirements such as high yields, high productivity, high selectivity and a good reaction control. In particular, it should provide a platform that is easy to operate by non-specialists, a modular setup to fit specific operating conditions and a robust design that's capable of an extended runtime. Furthermore it's also beneficial if the construction is easy and cheap. The most basic type of cell construction that is able to meet the specifications consists of an undivided setup with a solid electrode plate-to-plate geometry. Hence, this is the design the electrochemical microreactor is based upon with focus on a high specific electrode surface area and a low inter-electrode distance.

The reactor, which is schematically illustrated in Figure 1, consists of two parts which hold the electrodes. The electrodes are solid plates (Figure 1 no. 1) embedded with an epoxy resin in a PEEK (polyether ether ketone) housing Figure 1 no. 2). The PEEK material ensures an excellent chemical resistance to solvents and inorganic acids in the common concentrations as well as a high temperature resistance (if needed) and excellent adhesion to the epoxy resin. The PEEK housing has ports for the inlet and outlet of the flow channel and a threaded opening for the Ag/Ag^+ reference electrode (RE-7VP, ALS Co., Ltd, Japan). An electrical connection to the electrodes is glued with conductive silver epoxy in an opening in the back through which the electrodes are accessible. The electrodes are separated by a POM (polyoxymethylene) spacer in which the flow channel is machined (Figure 1 no. 3). The thickness of the spacer determines the distance between the electrodes (inter-electrode distance) and the reactor volume. In this work the spacer thickness is set to 4 mm giving a total reactor volume of 3.88 ml and a volume of 1.42 ml over the electrode for one channel in the divided setup. In order to achieve a good sealing, a groove was milled in the PEEK housing to incorporate an EPDM (ethylene propylene diene monomer rubber) O-ring which is compressed between the housing and the spacer. The two parts are held together in an aluminium holder which is secured by 14 bolts to 4 Nm (Figure 1 no. 4). The setup is easily and quickly dismantled and reassembled, unlike many designs reported in literature which are sealed completely. Swapping electrodes is done by using different housing parts in which other materials are embedded. A membrane can be incorporated in the reactor by fixing it between two identical spacers.

The electrolyte flow was provided by a HPLC pump (DeltaChrom P102 double piston pump). When a measurement is started it takes some time for a concentration profile to develop in the reactor which depends on the flow rate of the electrolyte. This is noticeable in the current response where initially a large current is observed which gradually decreases to a steady value. When steady state is reached, a sample is taken by filling a vial at the outlet. Each experiment is performed at least three times, unless specified otherwise.

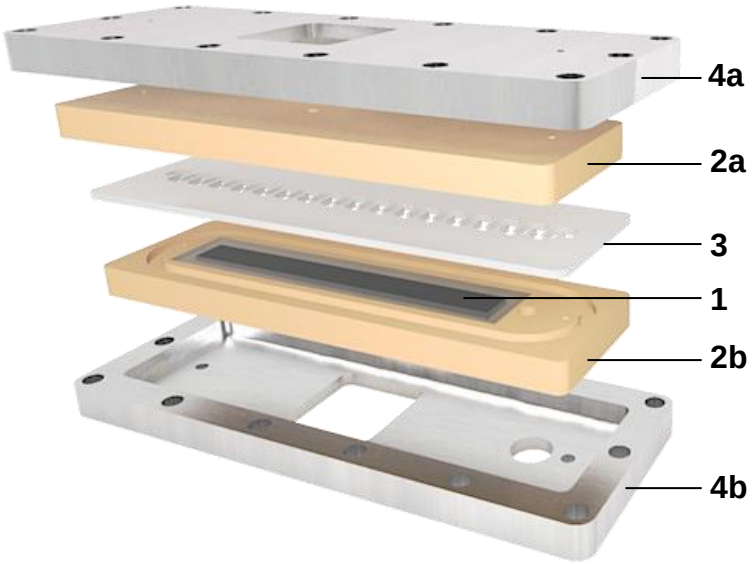

Figure 1: Exploded view of the electrochemical microreactor. 1: Electrode material embedded in the PEEK housing with epoxy resin. 2: PEEK housing with embedded electrode (2a: WE, 2b: CE), in- and outlet ports, reference electrode port (2b only), hole for the electrode connection and groove for the EPDM O-ring. 3: POM spacer with serpentine reaction channel. 4: Aluminium parts with holes for the in- and outlet tubing, hole for the reference electrode (4b only) and holes for the electrode connections.

2.3. Analysis

Analysis of the samples was performed by GC-FID (Thermo Scientific Trace 1300) on a polar capillary column (Restek RTX-Wax 30 m × 0.25 mm, PEG 0.25 µm). The carrier gas flow (He, 5.0 purity) was controlled at 1.4 ml/min. The temperature of the column was held constant at 40 °C for 1 minute and then ramped to 200 °C at 40 °C/min. This resulted in excellent separation of the target products allowing easy quantification. A calibration curve between 1 and 20 m% was established with a correlation coefficient of 0.9939. All samples were analysed at least three times with a standard deviation of no more than 5 % and usually much less.

2.4. Platinum deposition

The deposition of the platinum layers was done from a commercial plating solution (see 2.1) which is a 26×10^{-3} M solution of $Pt(NH_3)_4HPO_4$ in a dilute phosphate buffer (pH ~10.6). The deposition parameters were based on a literature report on plating bath conditions (Basirun et al., 1996). To optimise the deposition and characterise the deposited platinum layer, a solid copper disk electrode (d = 6 mm) was used as a substrate. For the working electrode in the reactor, a 10 × 1 × 0.6 cm copper plate embedded in a PEEK casing as described in 2.2 was used. Prior to the deposition the electrodes were mechanically polished (Struers LaboPol-

5) with 1 µm alumina slurry and rinsed with ultrapure water. The deposited platinum layer was also polished with subsequently 1, 0.3 and 0.05 µm alumina slurry and rinsed. The plating was performed in a three electrode configuration with a Pt counter electrode and Ag/AgCl reference electrode. For the reactor electrode, a special holder was machined and multiple platinum plate counter electrodes were combined and placed under the copper plate working electrode, covering the entire electrode. This ensures a uniform current distribution over the electrode so a uniform deposit is obtained. Several constant current and constant potential depositions were performed and the best results were obtained with a constant potential deposition at -720 mV vs. Ag/AgCl and at 365 K until a charge of 1 C cm^{-2} was passed. The high temperature has no direct influence on the deposited layer, but a limited influence on the efficiency and thus the rate of the deposition. A strict control of the temperature ensures a good reproducibility of the deposits. When glassy carbon (GC) was used as a substrate, visually identical platinum layer deposits were obtained but the deposited layers could easily be wiped off with the slightest touch. Contrarily the copper substrate depositions showed excellent adhesion and could only be removed by sanding down or polishing the electrode.

2.5. Determination of the global mass transfer

It is obvious that the spacer design influences the mass transfer of the electrochemical active species to the electrode surface, which is an important parameter with regards to the efficiency. In the electrosynthetic aldol reaction as performed, the electroactive species is the solvent itself, which is abundant at the electrode's surface. Hence, it could be said that mass transfer towards the electrode is of lesser interest. However, the radical species generated at the electrode are very reactive and increasing the mass transfer is important to prevent the reaction of the active species with the formed aldol which leads to further condensation products. In addition the increased mass transfer of the generated active radicals into the bulk increases the amount of possible radicals that can be formed, further increasing efficiency.

To evaluate the different designs of the spacers used in this work, the effect of the channel design on the mass transfer was investigated using the electrochemical limiting diffusion current technique. This technique and its application on micro- and minichannels is well documented in literature (Arenas et al., 2016; Ergu et al., 2009; Griffiths et al., 2005; Lira-Teco et al., 2016; Wilk, 2014). When the reaction is diffusion-controlled, the limiting current is given by:

$$I_{lim} = k_m n F A C_b \tag{1}$$

Where k_m is the global or mean mass transfer coefficient, n the number of the transferred electrons in the electrochemical reaction, F the Faraday constant and C_b the bulk concentration. If a well-known electrochemical system is used the mass transfer coefficient can easily be calculated from equation (1). In this work the reduction of ferricyanide to ferrocyanide is used.

The electrolyte used in the measurements consisted of 1×10^{-3} M potassium ferricyanide, 5×10^{-3} M potassium ferrocyanide and 0.5 M sodium sulphate as supporting electrolyte in ultrapure water. The electrodes in the reactor have the same dimensions, so to ensure that the limiting reaction is the cathodic reaction of ferricyanide, a 5 times higher concentration of ferrocyanide was used. The diffusion coefficient is 6.532×10^{-10} m^2 s^{-1} and the Schmidt number 1479 (Lira-Teco et al., 2016).

To perform the measurements, the inlet flow was held constant and the potential was stepped over a range. At each potential step the current was allowed to converge to a steady value before it was measured. This was done for a series of fixed values for the inlet flow.

3. Results and discussion

3.1. Characterisation and validation of the deposited platinum layer

From previous work from our group (Pauwels et al., 2016) it was established that, from a selected number of materials, platinum showed the best activity towards the aldol reaction of acetone as the equilibrium concentration is reached in the shortest amount of time. To incorporate platinum as a working electrode in the reactor, electrodeposition was used as a convenient and cost-effective method compared to using a solid platinum electrode. In case a larger surface area is desired, a similar deposition on a 3-dimensional electrode can be performed (Arenas et al., 2017). The depositions were performed as described in 2.4. Scanning electron microscopy (SEM) was used to characterise the surface of the deposited layer and a batch experiment was performed to compare the platinum deposit to a solid platinum disk electrode of equal size. For both aspects, the deposited platinum electrocatalyst performs similar to the bulk electrode (SEM images and data can be found in the supporting information).

3.2. Reactor setup

The aldol reaction is an indirect reaction initiated by an anionic species generated at the cathode. In an undivided batch setup the reaction is impeded by the cationic species generated by the anode, which can react with the anionic species generated at the cathode. An easy way to prevent this is to separate anode and cathode. Hence, the setup requires the use of a membrane to separate the electrodes adequately. The membrane used in this work is a commercial polypropylene microporous monolayer membrane (Celgard® 2500) with a thickness of 25 µm and 64 nm pores. When a membrane is incorporated in the reactor, attention should be given to the spacer design. The spacer channel was designed to ensure an easy definable laminar flow in the reactor. The most straightforward design is a rectangular channel such as spacer A in Figure 2. To increase the support of the membrane, a second spacer with a serpentine channel design was machined (Figure 2, spacer B). The bends in the reaction channel support the membrane. Both the total surface area of the reaction channel and the

accessible electrode surface area are slightly smaller for spacer B compared to spacer A. Therefore spacer B has a slightly smaller reactor volume at equal spacer thickness but still a similar electrode-surface-to-volume-ratio compared to spacer A. The surface area of the channel in spacer A is 1252 mm^2 and in spacer B 971 mm^2 while the length is 130 mm and 318 mm respectively. The spacer thickness is 4 mm in the undivided setup and 2 mm in the divided setup for each spacer with the membrane clamped in between. Both setups provide an inter-electrode distance of 4 mm. The thickness is arbitrary chosen and is set similar to the range of inter-electrode distances in commercially available microflow reactor setups such as the FM01-LC reactor and the ElectroCell A/S Micro Flow Cell (Rivera et al., 2015a).

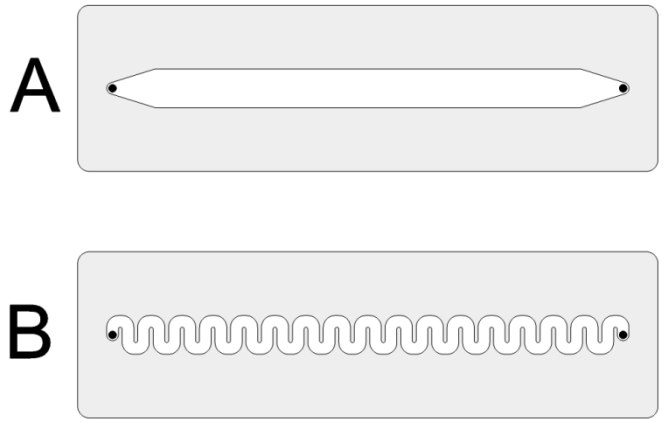

Figure 2: Representation of the spacer design, outer dimensions = 50 x 150 mm. Spacer A: rectangular channel with channel length = 130 mm and channel surface area = 1148 mm^2. B: serpentine channel with channel length = 318 mm and channel surface area = 971 mm^2. The dots represent the electrolyte inlet and outlet.

3.3. Evaluation of the spacer design

To evaluate the performance of both spacers, the global mass transfer was determined as described in section 2.5. A single spacer was used with a thickness of 4 mm. Measurements of the limiting current were performed for volumetric flow rates $\dot{V}$ = 0.5, 1, 2 and 3 ml min^{-1} which corresponds to a mean linear flow velocity of the electrolyte v = 0.18, 0.36, 0.73 and 1.09 mm respectively s^{-1} for spacer A and v = 0.50, 1.00, 1.99 and 2.99 mm s^{-1} for spacer B. Corresponding current-potential plots as illustrated in Figure 3 below are obtained.

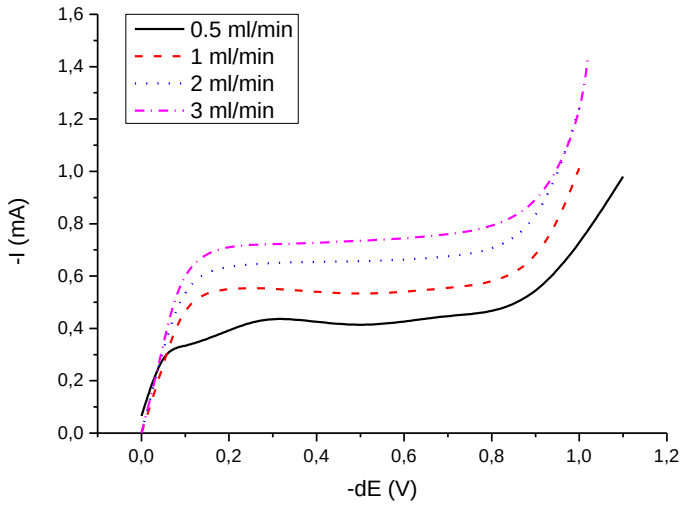

Figure 3: Current-potential plots of the limiting current region for the reduction of ferricyanide in the reactor with spacer A.

The plots show an initial steep increase of the current until a well-defined plateau is reached. This is the limiting current plateau from which the limiting current is derived. When the potential is stepped further, at a certain moment the current increases again, this is due to the onset of hydrogen evolution. For channel electrodes the limiting current is given by

$$I_{lim} = 0.925nFAC_bD^{2/3}\left(\frac{\dot{V}}{h^2d}\right)^{1/3} wx^{2/3} \quad (2)$$

Where *d* and *h* are respectively the channel width and half the channel height and *w* and *x* the electrode width and length. Equation (2) is valid when *h* << *d* and the electrode width *w* is sufficiently smaller than the channel width *d* to prevent edge effects. In addition the equation does not hold for sufficiently low flows or long electrodes as in such case, the Levêque approximation that is used (and in extension equation (2)) is no longer valid (Compton and Unwin, 1986). From (2) it is clear that for channel electrodes there is a linear correlation between the limiting current I_{lim} and the cube root of the flow rate $\dot{V}$. As explained in section 3.2, the spacer design and resulting reaction channel geometry doesn't represent an ideal channel electrode since the electrode width is equal to the channel width and the length is almost equal. Nevertheless plotting I_{lim} versus $\dot{V}^{1/3}$ gives a Pearson's correlation coefficient of 0.996 for spacer A and 0.892 for spacer B which indicates that the limiting current behaviour of the reactor for both spacers is still comparable to that of an ideal channel electrode.

From the limiting currents, the global mass transfer coefficients k_m were estimated using equation (1) and subsequently the Sherwood number *Sh* was calculated by:

$$Sh = \frac{k_m D_H}{D} \quad (3)$$

Where k_m is the global mass transfer coefficient, D_H is the hydraulic diameter and D the diffusion coefficient. The Sherwood number represents the ratio between the mass transfer by convection and mass transfer by diffusion and is the dimensionless version of the mass transfer coefficient. To characterise the performance of the spacers, *Sh* is plotted versus *Re* in Figure 4.

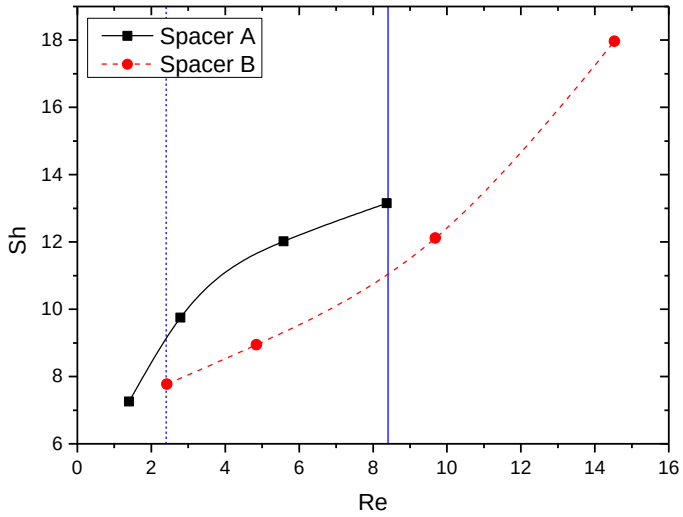

Figure 4: *Sh* versus *Re* plot for the two spacers. Squares connected by solid line: spacer A, dots connected by dashed line: spacer B. The horizontal lines mark the area of equal Re, which is referred to in Figure 5.

The fact that for the same volumetric flow rates the *Re* number for spacer B is higher than for spacer A is a logical consequence from the difference in aspect ratio and channel length between the two spacers. The hydraulic diameter is 40% less for spacer B compared to spacer A, but the channel length increases by more than 140%, which leads to higher fluid velocities (and thus *Re* numbers) for the same volumetric flow rates. A more interesting observation is that in the range of equal *Re* numbers, the mass transfer in spacer A is higher than in spacer B. To a certain extent, this is the consequence of the development of the flow profile, which can be checked by calculating the Graetz number as follows:

$$Gz = \frac{D_H}{L} ReSc \tag{4}$$

Where D_H is the hydraulic diameter, L the length and *Re* and *Sc* the well-known Reynolds and Schmidt numbers. A Graetz number of 20 or less (or $Gz^{-1} \geq 0.05$) is the point at which the flow profile is considered fully developed (Plawsky, 2001). A less developed flow profile has a thinner hydrodynamic boundary layer at the electrode surface and hence by extension, a beneficial effect on the mass transfer. This correlation is shown in Figure 5, where *Sh* is plotted versus Gz^{-1}. If *Gz* is calculated for a fixed length for both spacers in the range of overlapping *Re*, it is obvious from (4) that *Gz* for spacer A is higher than for spacer B for each value of *Re*, which is a direct

consequence of the difference in aspect ratio. This means that the flow profile is less developed in spacer A at equal channel lengths and equal *Re*, which contributes to a better mass transfer as explained above. However, even though spacer A shows a better mass transfer at equal *Re*, the higher fluid velocities for the same volumetric flow rate in spacer B compensate for this effect. So for the same electrode surface area and equal reactor volume, spacer B offers an equal or better mass transfer than spacer A for each volumetric flow rate. In addition spacer B offers a better support for the membrane, which prevents bending of the membrane that causes the possible blocking of one of the channels.

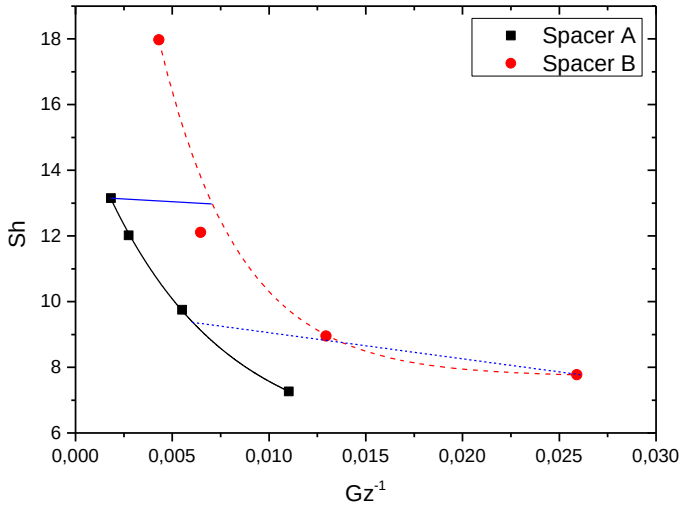

Figure 5: *Sh* versus Gz^{-1} plot for both spacers. Squares and solid line: experimental values and fitted curve for spacer A. Dots and dashed line: experimental values and fitted curve for spacer B. The horizontal lines represent the points of equal Re on both curves and correspond to the values marked by the vertical lines on Figure 4.

3.4. Electrochemical aldol reaction of acetone in a microfluidic reactor

The reaction is performed in the reactor setup as displayed in Figure 1. Spacer B is used to create the reaction channel and a membrane is incorporated to separate the electrodes with an inter-electrode distance of 4 mm. The counter electrode is a glassy carbon electrode and the reference electrode is Ag/Ag^+ (0.01 M $AgNO_3$). The reagent stream consists of acetone + 0.1 M n-Bu_4NClO_4. Two working electrodes are investigated: a catalytic platinum deposit and an inert glassy carbon electrode. Earlier work (Pauwels et al., 2016) showed that the reaction reaches an equilibrium concentration of approximately 15 m% DAA, the exact value varies a bit due to parameters such as temperature and dissolved oxygen. The fractional conversion is not explicitly calculated, but for all experiments, the selectivity is consistently very high (generally ≥95%) meaning that the fractional conversion correlates strongly to the yield of the product and in this case even is comparable in numerical value.

A flow rate of 0.5 ml min^{-1} corresponding to a mean linear flow rate of 0.50 mm s^{-1} was set. Figure 6 A shows that for this flow rate, both materials reach the same maximum equilibrium concentration of ±18 m% which corresponds to a space time yield of ρ_{ST} = 0.24 for Pt and 0.22 for GC. Decreasing the residence time would logically at one point cause the concentration (and consequently the yield) to drop. This effect is demonstrated in Figure 6 B which shows the results for an electrolysis of the same electrolyte in a smaller commercial thin layer cell with a platinum working electrode, which is used as a microfluidic reactor. The internal volume of the reactor is 36 µl and the surface area of the working electrode is7 mm^2 which gives it a similar electrode surface area to volume ratio than the constructed reactor reported in this work. The electrodes in this reactor are embedded in the same plane with a distance of 4 mm between them. This is a disadvantage because there is no possiblity to separate the electrodes giving it a worse performance than the constructed device. In Figure 6 B the normalized yield is plotted versus the residence time. Due to the smaller volume of the commercial reactor, much shorter residence times are achievable with the same pump installation. Figure 6 B clearly shows that for shorter residence times the concentration decreases and for longer residence times the concentration increases until the equilibrium concentration (or the maximum achievable concentration) in the given reactor setup is reached. From earlier results (Pauwels et al., 2016), it is known that in the same batch setup a GC electrode can also reach the maximum concentration as a Pt electrode does, but it takes a much longer electrolysis time, suggesting a lower activity for the reaction. Taken into account this difference, it is expected that the tipping point at which the equilibrium concentration is no longer achievable, is different for the two materials. Logically this would happen at a higher residence time for GC than for Pt. To evaluate to what extent the flow rate can be increased before this happens, the reaction is performed in a range of volumetric flow rates of 0.5 to 8 ml min^{-1} (the maximum flow rate of the pump), corresponding to mean linear flow rates of 0.50 to 7.96 mm s^{-1}. The results are also plotted in Figure 6 A. A first observation is that in the range of volumetric flow rates applied, taken the error bars into account, there is no significant difference in concentration that is obtained in the product stream between the different flow rates. A remark needs to be made on the noticeable decrease at a flow rate of 2 ml min^{-1}. This might suggest a pattern, however, this is more likely due experimental variation or error. A second observation is that within the measured range of flow rates there is no significant difference noticeable between the two electrode materials.

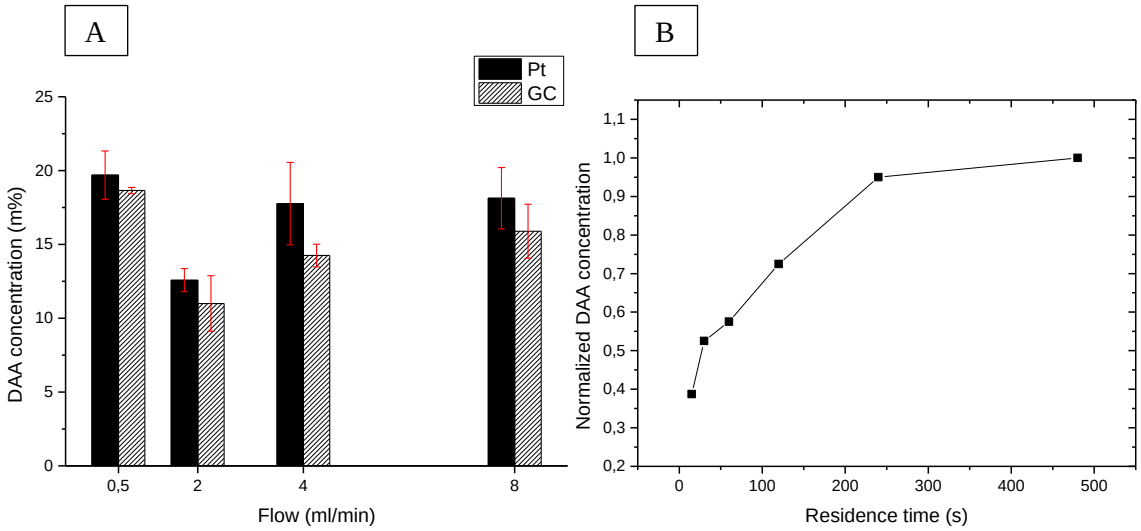

Figure 6: A: DAA concentration in the product stream at different volumetric flow rates in the reactor setup with a membrane with Pt (black columns) or GC (hatched columns) working electrode, GC counter electrode, electrolyte = acetone + 0.1 M TBAP, E = -2.35 V vs Ag/Ag^{+}, inter-electrode distance = 4 mm. Experiments performed in triplicate. B: normalised DAA concentration as a function of residence time for a platinum working electrode in a commercial microfluidic electrochemical reactor.

Figure 7 A shows a plot of the production rate capacity versus the flow rate for these experiments. Because similar concentrations are achieved at different flow rates, it is logical that a linear correlation exists (Pearson's r = 0.996 for Pt and 0.989 for GC) between the two. To compare the performance of the continuous flow reactor against the batch setup, the absolute yield for both is calculated for a time frame of two hours, which was the duration of the batch experiments. The electrode surface area in both setups is comparable as the difference between both is less than 10 % (8 cm^2 in the batch setup versus 7.3 cm^2 in the reactor setup with serpentine spacer). For the batch experiments an absolute yield of 11.9 g and a ρ_{ST} =0.0085 mmol cm^{-3} min^{-1} was achieved after this time while for the reactor, in the best conditions in these experiments, the total amount of DAA was 68.8 g and ρ_{ST} = 3.04 mmol cm^{-3} min^{-1}, which is almost a six fold increase in absolute yield and 300 fold increase in space time yield. The continuous replenishing of reactant in proximity of the electrode and the large electrode surface area to volume ratio has a significant beneficial effect on the DAA production.

Another parameter that is checked is the apparent current efficiency, for which an interesting observation is notable. From the current curves which are recorded during the experiment (not shown), it is clear that for the glassy carbon working electrode the current density rises less than linear with increasing flow rate, increasing from 0.60 mA cm^{-2} at 0.5 ml min^{-1} to 0.95 mA cm^{-2} at 8 ml min^{-1}. This means that the faradaic efficiency increases with the flow rate as the production capacity rate does increase linearly with the flow rate. This is obvious in Figure 7 B where the yield per charge passed increases from 0.14 g C^{-1} at 0.5 ml min^{-1} to 1.20 g C^{-1} at 8 ml min^{-1} which is a tenfold increase in current density but a 16 fold increase in volumetric flow rate (or mean linear flow

rate). In the batch setup, glassy carbon after two hours had an overall efficiency of 0.34 g C^{-1}, which is higher than the efficiencies obtained in the reactor at 0.5 and 2 ml min^{-1}, but much lower than the efficiencies at 4 and 8 ml min^{-1}. Higher flow rates might prevent certain side reactions taking place on the glassy carbon electrode, increasing its efficiency. In addition, faster removal of DAA from the electrogenerated base limits the reverse reaction, leading to a higher apparent current efficiency.

For the platinum deposit working electrode the current density in the reactor increases linearly from 0.93 mA cm^{-2} at 0.5 ml min^{-1} to 4 mA cm^{-2} at 2 ml min^{-1} and then remains constant around that value for higher flow rates. Consequently the efficiency increases only slightly from 0.10 g C^{-1} at 0.5 ml min^{-1} to 0.33 g C^{-1} at 8 ml min^{-1}. The value of 0.33 g C^{-1} is comparable to the divided batch setup with a platinum working electrode where the efficiency was 0.35 g C^{-1} after two hours. The faradaic loss for the platinum deposit working electrode is not completely clear, but is probably related to gas evolution (possibly hydrogen evolution). This is noticeable during operation where gas bubbles are visible in the outlet tubing on the cathodic side. The formation of these bubbles not only lowers the faradaic efficiency, but also leads to possible blocking of the electrode, reducing the available electrode surface area. The formation of gaseous products on the anodic side is not observed and for a glassy carbon working electrode, no gaseous products are observed at all. In the range of flow rates measured, the same concentration is reached on both materials up to the highest flow rate. This gives glassy carbon a better performance than platinum due to the higher efficiency. In the batch setup the efficiency of both materials was comparable while the activity of platinum was much higher, resulting in a higher yield. However, further lowering residence time will most probably lower the maximum obtainable concentration as seen in Figure 6 B and this presumably happens at a longer residence time for glassy carbon than for platinum. A parameter which plays a role here is the inter-electrode distance. A smaller distance can have a beneficial effect on the total power input of the setup due to the decreasing ohmic losses between the two electrodes (which can be quite large in non-aqueous solvents). However, this also decreases the total volume and thus for the same volumetric flow rates, the residence time decreases. This has its effect on the space-time yield and the absolute yield. Optimisation depends on tuning the setup to find a balance between yield and efficiency. The fact that for this configuration up until the highest applicable flow rate the maximum concentration is achieved on both materials, highlights the ease by which this reaction can be performed in an electrochemical microreactor.

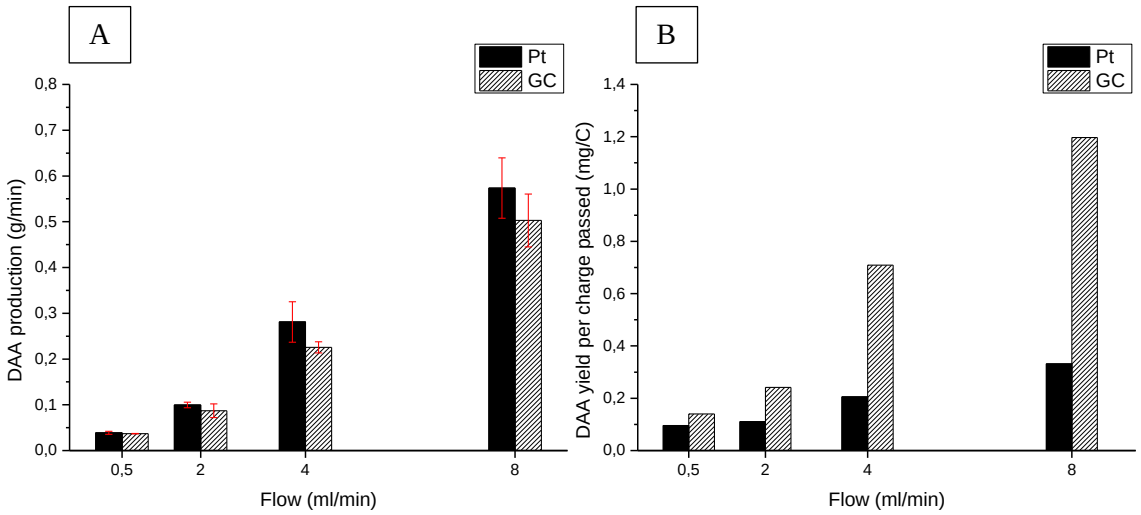

Figure 7: A: DAA yield per minute versus volumetric flow rate. B: Apparent efficiency (yield per charge passed) versus volumetric flow rate.

4. Conclusions

The electrosynthetic aldol reaction of acetone to diacetone alcohol was performed in an electrochemical microfluidic reactor. The reactor design was focused on a modular, robust setup which is easy to (dis)assemble and to operate. The implementation of a membrane was necessary to prevent the mixing of electrogenerated species which has a negative impact on the reaction. Due to the modular setup, inserting or removing a membrane is fast and easy. To prevent blocking of the electrode chambers caused by bending of the membrane, a spacer with serpentine flow channel was used to support the membrane. This spacer, while providing nearly the same available electrode surface area and reactor volume as a similar sized rectangular flow channel, has a beneficial effect on the mass transfer in the reactor due to the increased channel length. In the divided setup, a maximum productivity of 0.57 g min^{-1} of DAA (ρ_{ST} = 3.04 mmol cm^{-3} min^{-1}) at an efficiency of 0.33 g C^{-1} was achieved on a platinum working electrode at -2 V vs Ag/AgCl and a volumetric flow rate of 8 ml min^{-1} (7.96 mm s^{-1}), which is a six fold increase compared to the batch setup reported earlier. Even at the maximum flow rate of the pump, the reactor is still not operating at the point where the maximum obtainable DAA concentration is less than the equilibrium concentration. Therefore no significant difference in DAA production rate capacity or concentration was noticeable between the two electrode materials tested. However, preliminary tests in a smaller commercial setup showed that at sufficiently low residence times, the productivity decreases faster (at longer residence times) for glassy carbon than for platinum. The efficiency of platinum of 0.33 g C^{-1} in the reactor setup is similar to the 0.35 g C^{-1} in batch setup. This efficiency is limited due to the gas formation on the platinum electrode and the lack thereof on the glassy carbon electrode gives it a better efficiency as platinum in the reactor setup. Though further optimisation of the electrode surface area and the reactor volume for a maximum

productivity is still possible, it has been demonstrated that the application of a simple electrochemical microreactor for the aldol reaction of acetone to diacetone alcohol leads to a high rate of product formation, a high selectivity and a high current efficiency. Furthermore, the microreactor setup combines the advantages of electrosynthesis with those of flow chemistry and offers an stable, robust and easy to scale up system. These promising results provide a next step for the implementation of electrosynthesis in an industrial application as a green and clean alternative for the existing chemical processes.

Acknowledgements

The authors would like to thank Bert De Mot for assisting with the measurements. Jonas Hereijgers greatly acknowledges the Research Foundation - Flanders (FWO) for support through a Post-Doctoral grant (12Q8817N).

References

Arenas, L.F., de León, C.P., Boardman, R.P., Walsh, F.C., 2017. Electrodeposition of Platinum on Titanium Felt in a Rectangular Channel Flow Cell. J. Electrochem. Soc. 164, D57–D66. doi:10.1149/2.0651702jes

Arenas, L.F., Leon, C.P. de, Walsh, F.C., 2016. Mass transport and active area of porous Pt/Ti electrodes for the Zn-Ce redox flow battery determined from limiting current measurements. Electrochim. Acta 221, 154–166. doi:10.1016/j.electacta.2016.10.097

Basirun, W.J., Pletcher, D., Saraby-Reintjes, A., 1996. Studies of platinum electroplating baths Part IV : Deposits on copper from Q bath. J. Appl. Electrochem. 26, 873–880. doi:10.1007/BF00683750

Compton, R.G., Unwin, P.R., 1986. Channel and tubular electrodes. J. Electroanal. Chem. Interfacial Electrochem. 205, 1–20. doi:10.1016/0022-0728(86)90219-6

Ergu, O.B., Sara, O.N., Yapici, S., Arzutug, M.E., 2009. Pressure drop and point mass transfer in a rectangular microchannel. Int. Commun. Heat Mass Transf. 36, 618–623. doi:10.1016/j.icheatmasstransfer.2009.03.015

Green, R., Brown, R., Pletcher, D., 2014. Understanding the Performance of a Microfluidic Electrolysis Cell for Routine Organic Electrosynthesis. J. Flow Chem. 5, 31–36. doi:10.1556/JFC-D-14-00027

Griffiths, M., De León, C.P., Walsh, F.C., 2005. Mass transport in the rectangular channel of a filter-press electrolyzer (the FM01-LC reactor). AIChE J. 51, 682–687. doi:10.1002/aic.10311

Horcajada, R., Okajima, M., Suga, S., Yoshida, J., 2005. Microflow electroorganic synthesis without supporting electrolyte. Chem. Commun. 1303–1305. doi:10.1039/b417388k

Horii, D., Fuchigami, T., Atobe, M., 2007. A New Approach to Anodic Substitution Reaction Using Parallel Laminar Flow in a Micro-Flow Reactor. J. Am. Chem. Soc. 11692–11693.

Keefe, W.K.O., Jiang, M., Ng, F.T.T., Rempel, G.L., 2005. Liquid phase kinetics for the selective hydrogenation of mesityl oxide to methyl isobutyl ketone in acetone over a Pd / Al 2 O 3 catalyst. Chem. Eng. Sci. 60, 4131–4140. doi:10.1016/j.ces.2005.02.049

Kirschner, E.M., 1994. Environment, Health Concerns Force Shift In Use Of Organic Solvents. Chem. Eng. News 72, 13. doi:10.1021/cen-v072n025.p013

Küpper, M., Hessel, V., Löwe, H., Stark, W., Kinkel, J., Michel, M., Schmidt-Traub, H., 2003. Micro reactor for electroorganic synthesis in the simulated moving bed-reaction and separation environment. Electrochim.

Acta 48, 2889–2896. doi:10.1016/S0013-4686(03)00353-0

Lira-Teco, J.E., Rivera, F., Farías-Moguel, O., Torres-González, J., Reyes, Y., Antaño-López, R., Orozco, G., Castañeda-Zaldivar, F., 2016. Comparison of experimental and CFD mass transfer coefficient of three commercial turbulence promoters. Fuel 167, 337–346. doi:10.1016/j.fuel.2015.11.053

Marshall, R.J., Walsh, F.C., 1985. A review of some recent electrolytic cell designs. Surf. Technol. 24, 45–77. doi:10.1016/0376-4583(85)90015-9

Paddon, C.A., Atobe, M., Fuchigami, T., He, P., Watts, P., Haswell, S.J., Pritchard, G.J., Bull, S.D., Marken, F., 2006. Towards paired and coupled electrode reactions for clean organic microreactor electrosyntheses. J. Appl. Electrochem. 61, 617–634. doi:10.1007/s10800-006-9122-2

Paddon, C.A., Pritchard, G.J., Thiemann, T., Marken, F., 2002. Paired electrosynthesis : micro-flow cell processes with and without added electrolyte. Electrochem. commun. 4, 825–831.

Pauwels, D., Hereijgers, J., Verhulst, K., De Wael, K., Breugelmans, T., 2016. Investigation of the electrosynthetic pathway of the aldol condensation of acetone. Chem. Eng. J. 289, 554–561. doi:10.1016/j.cej.2016.01.018

Pickett, D.J., 1979. Electrochemical Reactor Design, 2nd ed. Elsevier, Amsterdam.

Plawsky, J.L., 2001. Transport phenomena fundamentals.

Pletcher, D., Walsh, F.C., 1990. Industrial Electrochemistry, 2nd ed. Chapman and Hall, London.

Rivera, F.F., De León, C.P., Nava, J.L., Walsh, F.C., 2015a. The filter-press FM01-LC laboratory flow reactor and its applications. Electrochim. Acta 163, 338–354. doi:10.1016/j.electacta.2015.02.179

Rivera, F.F., León, C.P. De, Walsh, F.C., Nava, J.L., 2015b. The reaction environment in a filter-press laboratory reactor: The FM01-LC flow cell. Electrochim. Acta 161, 436–452. doi:10.1016/j.electacta.2015.02.161

Rode, S., Attour, A., Lapicque, F., Matlosz, M., 2008. Thin-Gap Single-Pass High-Conversion Reactor for Organic Electrosynthesis. J. Electrochem. Soc. 155, 193–200. doi:10.1149/1.2996568

Scialdone, O., Galia, A., Sabatino, S., Vaiana, M., Agro, D., Busacca, A., Amatore, C., 2014. Electrochemical Conversion of Dichloroacetic Acid to Chloroacetic Acid in Conventional Cell and in Two Microfluidic Reactors. ChemElectroChem 5, 116–124. doi:10.1002/celc.201300216

Scialdone, O., Guarisco, C., Galia, A., 2011. Oxidation of organics in water in microfluidic electrochemical reactors: Theoretical model and experiments. Electrochim. Acta 58, 463–473. doi:10.1016/j.electacta.2011.09.073

Watts, K., Baker, A., Wirth, T., 2014. Electrochemical Synthesis in Microreactors. J. Flow Chem. 4, 2–11. doi:10.1556/JFC-D-13-00030

Wendt, H., Kreysa, G., 1999. Electrochemical Engineering. Springer-Verlag, Berlin.

Wilk, J., 2014. A review of measurements of the mass transfer in minichannels using the limiting current technique. Exp. Therm. Fluid Sci. 57, 242–249. doi:10.1016/j.expthermflusci.2014.04.019

Ziogas, a., Kolb, G., O'Connell, M., Attour, a., Lapicque, F., Matlosz, M., Rode, S., 2009. Electrochemical microstructured reactors: design and application in organic synthesis. J. Appl. Electrochem. 39, 2297–2313. doi:10.1007/s10800-009-9939-6